

# Optimisation of the Magnetocaloric Effect in Low Applied Magnetic Fields in $LnOHCO_3$ Frameworks

Richard J.C. Dixey<sup>†</sup> and Paul J. Saines<sup>\*†</sup>

<sup>†</sup>School of Physical Sciences, Ingram Building, University of Kent, Canterbury, CT2 7NH, UK.

*Supporting information*

---

This study probes the structure and magnetocaloric effect of the  $LnOHCO_3$  ( $Ln = Gd^{3+}$ ,  $Tb^{3+}$ ,  $Dy^{3+}$ ,  $Ho^{3+}$  and  $Er^{3+}$ ) frameworks. A combination of single crystal X-ray and neutron powder diffraction indicate that these materials solely adopt the  $P2_12_12_1$  structure under these synthetic conditions and magnetic susceptibility measurements indicate they remain paramagnetic down to 2 K. We show that the magnetocaloric effect of  $TbOHCO_3$  and  $DyOHCO_3$  have a peak entropy change of 30.99 and 33.34 J K<sup>-1</sup> K<sup>-1</sup> for a 2-0 T field change respectively, which is higher than than the promising  $GdOHCO_3$  framework above 4 K in moderate magnetic fields. The magnetic entropy change of  $TbOHCO_3$  and  $DyOHCO_3$  above 4 K for sub-2T field changes also exceeds that of  $Gd_3Ga_5O_{12}$  and  $Dy_3Ga_5O_{12}$ , making them suitable magnetic cooling materials for use at liquid helium temperatures using the low applied magnetic fields accessible using permanent magnets, advantageous for efficient practical cooling devices.

---

## 1. INTRODUCTION

The magnetocaloric effect (MCE) is an entropically driven cooling process that occurs when paramagnets are in a cycled magnetic field<sup>1</sup>. Lanthanide ions are most suited to MCE materials, having the largest number of unpaired spins and greatest magnetic moment. The maximum magnetic entropy change ( $-\Delta S_m$ ) is usually assumed to be  $nR\ln(2S+1)$ , which neglects any contribution from the angular orbital momentum.<sup>2-4,5</sup> For this reason  $Gd^{3+}$  materials have traditionally been favoured as magnetocaloric materials as they have the largest entropy per single ion with exactly half filled  $f$ -orbitals ( $S=7/2$ ). They are optimized at sub 2 K temperatures for uses, where reaching millikelvin temperatures is priority over energy efficiency, and requiring large fields with superconducting magnets have been deemed acceptable.

The efficiency of MCE cooling can be greatly improved by developing materials that provide large changes of entropy in low fields (below 2 T), allowing them to be used in conjunction with a permanent magnet rather than relying on the use of superconducting magnets<sup>6</sup>. If such optimisation of MCE properties at low applied fields is coupled with an increase in temperature at which the MCE effect peaks to above 4 K, this approach could potentially be used for cooling at liquid He temperatures. This has a greater range of applications than cooling below 2 K, including for cooling superconducting magnets in devices such as medical resonance imaging (MRI) scanners and NMRs. Such applications typically rely on liquid helium, which is becoming an increasingly scarce, expensive and vital resource.<sup>7</sup> While cryogen free cryocoolers are available as alternatives for cooling to the liquid He temperature regime their efficiency at such temperatures is particularly low, typically only a couple of percent<sup>8</sup>. It is therefore important to investigate if MCE materials can be optimized to have high performance in low applied magnetic fields between 4 and 20 K. Such materials could then be used for cooling in the liquid He regime likely in conjunction with, more efficient, higher temperature cryocoolers.<sup>9,10</sup>

For such optimisation of MCE materials, it is becoming apparent that it is important to not just achieve a high density of magnetic cations but also control the magnetic interactions in these compounds. It is well established that frustrated magnetic interactions can enhance MCE behaviour, including in the benchmark oxide  $Gd_3Ga_5O_{12}$ ,<sup>11-13</sup> frustrated interactions enable a higher density of magnetic cations to be incorporated in a phase that remains paramagnetic to low temperature than is possible in the alternative “dilute” magnetic salts, which depend on having well separated magnetic centres to remain paramagnetic<sup>14</sup>. As a result, magnetic frustration increases the maximum  $-\Delta S_m$  possible per unit volume or weight. It has also been shown that the Ising-like interactions in  $Dy_3Ga_5O_{12}$  play a role in it having superior MCE performance for field changes below 2 T than found in  $Gd_3Ga_5O_{12}$ ;<sup>15</sup> this concept is supported by similar improvement in the MCE properties of other families of compounds when Gd is substituted with lanthanides with Ising-like interactions.<sup>16-18</sup> Amongst such Ising-systems  $Tb(HCO_3)_3$  is particularly promising as a MCE material for use in low applied fields above 4 K; this has been suggested to be linked to the existence of strong 1D ferromagnetic correlations in this material enabling its magnetic moments to align even more easily with applied magnetic fields.<sup>18,19</sup>

These results provide a drive for examining MCE materials based on other late lanthanides, including Tb and Dy particularly in structures supportive of frustrated and low dimensional magnetism. An obvious starting point for such studies is families in which the Gd analogue is already known to have promising MCE properties.  $GdPO_4$ ,  $GdOHCO_3$  and  $GdF_3$  have been shown to have some of the largest peak MCE yet<sup>6,13,20</sup>, with  $-\Delta S_m$  of ~58, 69.3 and 67.4 J kg<sup>-1</sup> K<sup>-1</sup> at 2 K for a 5-0 T field changes, respectively, compared to x for  $Gd_3Ga_5O_{12}$ . Notably of these high performance families two are dense coordination frameworks, which contain polyatomic anions. Such frameworks tend to adopt highly anisotropic structures with a range of conflicting magnetic interactions between magnetic cations.<sup>6,21,22,23</sup> The  $LnOHCO_3$  frameworks appear particularly interesting as they have a

conceptually similar structure to the  $Ln(\text{HCO}_2)_3$ , as it can be viewed as having 1D chains packed in a triangular lattice with previous calculations suggesting the presence of competing antiferromagnetic interchain coupling.

Inspired by the recent success of  $\text{Tb}(\text{HCO}_2)_3$  MCE in low fields and at temperatures above 2 K<sup>18</sup>, we therefore present a study of  $Ln\text{OHCO}_3$  paramagnetic MCE materials (where  $Ln$  = lanthanide) in magnetic fields up to 5 T. We have synthesized and structurally characterized a family of these materials using a combination of powder and single crystal diffraction, focusing on the heavier lanthanides due to their high magnetic moments as required for greater MCE. Finding that under moderate hydrothermal conditions these form  $P\bar{6}$  hexagonal crystal structures for Pr, Nd and Sm and  $P2_12_12_1$  monoclinic structures for the later lanthanides, which has previously been debated.<sup>23–26</sup> Their magnetic properties have also been characterized with a focus on the magnetocaloric properties of the later lanthanides between Tb and Er. We find that  $\text{TbOHCO}_3$  and  $\text{DyOHCO}_3$  are exceptional MCE materials above 4 K, both surpassing the peak MCE of the benchmark magnetic cooler  $\text{Gd}_3\text{Ga}_5\text{O}_{12}$  (GGG) observed at much lower temperature in the lower applied fields accessible using permanent magnets<sup>27</sup>;  $\text{DyOHCO}_3$  is particularly promising having the highest performance in the 4–10 K temperature range. Doping of  $\text{Gd}^{3+}$  into  $\text{TbOHCO}_3$  or  $\text{DyOHCO}_3$  has also been explored and while good stoichiometric control has been achieved this does not result in improved MCE, in contrast with the  $Ln(\text{HCO}_2)_3$  frameworks. These results highlight that the MCE is not only determined by the magnetic ion, but that structural and ligand field effects can contribute greatly to this behaviour.

## 2. EXPERIMENTAL SECTION

$Ln(\text{NO}_3)_3 \cdot x\text{H}_2\text{O}$  were synthesized by mixing (where  $x = 6$  for  $Ln = \text{Pr, Nd, Sm-Tb}$ , and  $x = 5$  for  $\text{Dy-Er}$ ) (1.0 mmol) (99.9%, Sigma-Aldrich) and  $\text{Na}_2\text{CO}_3$  (99.5% Fischer-Scientific) (1.0 mmol) in deionized  $\text{H}_2\text{O}$  (10 mL). The mixture was sealed in a Teflon-lined (23 mL) Parr-Bomb autoclave and heated at 170°C (150°C for  $\text{SmOHCO}_3$ ) for 72 h, followed by cooling to room temperature at a rate of 3°C h<sup>-1</sup>. Polycrystalline samples were obtained for  $Ln = \text{Pr, Nd Sm-Gd}$  and  $\text{Dy-Er}$ , and small single crystals obtained for  $\text{TbOHCO}_3$ . The samples were isolated by vacuum filtration and washed with deionized water.  $Ln\text{ODCO}_3$  samples used for neutron diffraction measurements were prepared with  $\text{D}_2\text{O}$  (99.9 %) under a  $\text{N}_2$  atmosphere.

Sample phase purity was examined by powder X-ray diffraction measurements performed on ground polycrystalline samples on either an Emperean PANalytical or a Rigaku MiniFlex with  $\text{Cu K}\alpha$  radiation with the use of a zero-background silicon sample holder. X-ray patterns with Rietica<sup>28</sup> using the Le Bail fitting method (ESI Figures S1–5).

Powder neutron diffraction measurements were carried out on the high-resolution time-of-flight (TOF) WISH diffractometer at the ISIS neutron source, Rutherford Appleton Laboratory.  $\text{TbODCO}_3$ ,  $\text{HoODCO}_3$  and  $\text{ErODCO}_3$  were loaded into 8mm vanadium cans, and  $\text{DyODCO}_3$  was loaded into a 6mm vanadium can. Measurements were carried out down to 1.5 K with the sample cooled using the standard low-background <sup>4</sup>He cryostat utilized on the beamline. Neutron patterns were fitted in GSAS<sup>29</sup> via the EXPGUI<sup>30</sup> interface with the Rietveld method. A Shifted Chebyshev model was used to fit the background of the measurements and using a profile function built from a convolution of back-to-back exponentials with a pseudo-Voigt function TOF to fit the peak shapes.

Single-crystal diffraction data was recorded on a Rigaku Supernova with  $\text{Mo K}\alpha$  radiation ( $\lambda = 0.7107 \text{ \AA}$ ) generated from a

microfocus source, operating at 0.8 kV and 50 mA, with multi-layer focusing optics. The sample was held in a MiTeGen micro-loop and cooled to 169 K using an Oxford Cryosystem. The data obtained was indexed, integrated and reduced using the CrysAlisPro software suite version 1.171.38.41<sup>31</sup>, with empirical absorption corrections performed using the same packages. The structure was solved using the Patterson method in SHELXS-2008<sup>32</sup> and refinements subsequently carried out using a least-squares method with SHELXL-2015<sup>33</sup> using the Olex2 graphical user interface<sup>34</sup>. Only the atomic displacement parameters for Tb were refined anisotropically, with lighter elements refined isotropically as the quality of the fit is insensitive to these values. The hydrogen atom positions were determined from the Fourier difference and refined with a restraint that it remains 0.96 Å from the oxygen to which it is attached and its displacement parameters constrained to be 1.5 times the oxygen that it is attached to (See Table 1 for crystallographic details).

**Table 1. Crystallographic data for the structure of  $\text{TbOHCO}_3$  determined by single crystal X-ray diffraction.**

Compound	$\text{TbOHCO}_3$
Formula	$\text{TbCHO}_4$
Formula Weight	235.94
$T$ (K)	169(2)
Crystal System	Orthorhombic
Space Group	$P2_12_12_1$
$a$ (Å)	4.8551(2)
$b$ (Å)	7.0178(3)
$c$ (Å)	8.4394(4)
$V$ (Å <sup>3</sup> )	287.55(2)
$Z$	4
$\rho_{\text{cal}}$ (g cm <sup>-3</sup> )	5.450
$\mu$ (cm <sup>-1</sup> )	24.402
Refl. meas./unique	2063/710
Parameters refined	33
$R_1, wR_2^a$ (all)	0.0400, 0.0776
$R_1, wR_2^a$ (obs)	0.0341, 0.0725
Goodness of Fit	1.062

$$^a \quad w = 1/[\sigma^2(F_o^2) + (aP)^2 + bP] \quad \text{and} \quad P = (\max(F_o^2, 0) + 2F_c^2)/3;$$

$$R_1 = \sum ||F_o| - |F_c|| / \sum |F_o| \quad \text{and} \quad wR_2 = \sqrt{[(F_o^2 - F_c^2) / \sum w(F_o^2)]^2}$$

The magnetic measurements of the polycrystalline samples (15–20 mg) were performed using a Quantum Design MPMS SQUID magnetometer. Samples were placed in gelatin capsules enclosed inside a pierced straw with a uniform diamagnetic background. Zero field cooled (ZFC) and field cooled (FC) measurements were recorded in a DC field 2–300 K for  $Ln\text{OHCO}_3$  (where  $Ln = \text{Pr, Nd Sm-Er}$ ) in 1000 Oe field, results did not show any indication of long range order. Field sweeps used to calculate entropy using Maxwell relations was measured 2–12 K in a DC field and fields 0–50 kOe, with varying intervals.

The thermal stabilities were characterized with a Netzsch STA 409 per TGA-DSC between 20–800 °C, heating at a rate of 10° min<sup>-1</sup> with data analysed using Netzsch Proteus. The infrared absorption spectrum of these samples was recorded with a Shimadzu IRAffinity-1 Fourier transform infrared spectrometer in the range 500–4000 cm<sup>-1</sup>, and analysed with LabSolutions IR.

## 3. RESULTS AND DISCUSSION

## Crystal Structures and Thermal Stability of the $LnOHCO_3$ Frameworks

$LnOHCO_3$  are known to form as different polymorphs in at least 2 different space groups  $P\bar{6}$ , most commonly adopted at higher synthetic pressures, and orthorhombic space group(s)  $Pnma$  or  $P2_12_12_1$ , which typically form at lower synthetic pressure<sup>25</sup>. The  $P\bar{6}$  polymorph is distinctly different from the other two reported structures, having a much larger unit cell. In our study it is found to only be adopted by the larger lanthanides, Pr and Nd.  $SmOHCO_3$  made at 170°C is a mixed phase of hexagonal and orthorhombic structures but lowering the hydrothermal temperature to 150°C forms a pure orthorhombic phase. The heavier lanthanides Gd-Er were only found to adopt orthorhombic structures so, since they are more likely to have the significantly magnetocaloric properties of interest to this study, the rest of this section will focus on distinguishing which of the two possible orthorhombic structures they adopt.

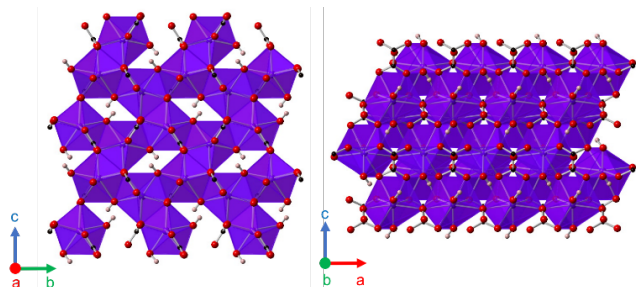


**Figure 1.** Polyhedral models of  $LnOHCO_3$  in  $P2_12_12_1$ , a) (100 plane) and b) (010) plane.  $LnO_{10}$  polyhedral in purple and oxygen, carbon and hydrogen atoms in red black and pink, respectively.

The  $Pnma$  and  $P2_12_12_1$  structures are very similar; the  $P2_12_12_1$  structure has 4 unique oxygen atoms, one for the hydroxide groups and three distinct oxygen atoms in the carbonate anions while the  $Pnma$  structure has 3 unique oxygen atoms, with two oxygen atoms in each carbonate anion being related by symmetry with fractional hydrogen occupation. The only other significant difference between the two structures is that the identity of the  $a$  and the  $b$  axis are reversed in their conventional settings. In both, the lanthanide can be viewed as being 10 coordinate with chains of  $LnO_{10}$  face-sharing polyhedra, with edge-sharing inter-chain connectivity. Alternatively, if the longest two bonds in the  $LnO_{10}$  polyhedra are neglected, which are 0.1-0.2 Å longer than other  $Ln-O$  bonds in this structure, it can be simplified as consisting of highly distorted  $LnO_8$  square antiprisms; these can in turn be viewed as being packed into edge-sharing  $LnO_8$  chains connected by oxygen atoms from the carbonate ligands with corner-sharing interchain connectivity via the hydroxide groups. Either of these simplifications of this complex structure feature low-dimensional motifs, shown to be linked with low-field high performance magnetocalorics, with previous calculations indicating intrachain coupling is dominant.<sup>19,23</sup>

We have been able to synthesize single crystal of  $TbOHCO_3$  and the single crystal structures determined from these have  $P2_12_12_1$  orthorhombic symmetry, with systematic absences required for the  $Pnma$  structure clearly violated. Single crystals were not, however, available from the other members of this series. Powder X-ray diffraction patterns of the two possible orthorhombic polymorphs produce almost identical patterns because the weak reflections indicating violation of  $Pnma$  symmetry are below the background of the instruments used in this study even for longer measurements. While distinguishing between these two polymorphs is therefore difficult using powder X-ray diffraction the greater sensitivity of neutron diffraction to the positions of

light atoms, such as the oxygen atoms that are the primary difference between these two structures, enables this to clearly distinguish between these two possibilities.

The neutron diffraction patterns we have measured on  $LnODCO_3$  ( $Ln = Tb-Er$ ) samples on the WISH neutron diffractometer clearly all show reflections that violate the systematic absences expected for the  $Pnma$  space group confirming that all samples adopt the  $P2_12_12_1$  space group. This is most clearly highlighted by a weak reflection observed at a  $d$ -spacing of about 3.18 Å (the (102) reflection in  $P2_12_12_1$ ) in all diffraction patterns of these compounds, which is allowed by  $P2_12_12_1$  symmetry but not in  $Pnma$  where this is the (012) reflection (see Figure 2). These structures remain in the  $P2_12_12_1$  space group for all temperatures recorded between 1.5-100 K for all four compounds studied. Additional diffraction patterns of  $TbOHCO_3$  and  $ErOHCO_3$  obtained at 300 K indicate these materials retain  $P2_12_12_1$  symmetry up to ambient conditions. Given Tb and Er are the largest and smallest lanthanides, respectively, hosted in the series of compounds studied by neutron diffraction, we suggest that none of these compounds have any structural phase transitions between 1.5-300 K retaining  $P2_12_12_1$  throughout this temperature range. This precludes the possibility of observations of a  $Pnma$  polymorph due to structural phase transition up to ambient temperature in these four compounds (ESI Figures S6-25). Unfortunately, due to its high neutron absorption cross section it is not possible to use neutron diffraction to directly study the Gd member of this series, although it is likely it adopts the same structure as found for Tb-Er, at least under the synthetic conditions used in this study. Bond distances determined by Rietveld refinements of neutron diffraction data can be seen in the ESI, and bond valence sums<sup>35</sup> were determined to be consistent with trivalent oxidation states for Tb, Dy, Ho and Er in  $LnODCO_3$ ; values of 3.12, 3.14, 3.10 and 3.16 respectively, were obtained.

Doping  $Tb^{3+}$  and  $Dy^{3+}$  with  $GdOHCO_3$ , to produce  $Tb_xGd_{1-x}OHCO_3$  and  $Dy_xGd_{1-x}OHCO_3$  frameworks, was successful with stoichiometric control over doping confirmed from the unit cell volume change consistent with Vegard's law (ESI Figures S26-29). The trend in unit cell volume obtained to fits from powder X-ray diffraction patterns suggest stoichiometries of  $x = 0.18, 0.37, 0.63, 0.81$  for Tb and  $x = 0.22, 0.40, 0.60, 0.77$  for Dy have been achieved, close to the nominal stoichiometries.

TGA studies of  $LnOHCO_3$  have shown the frameworks to be stable until around 450°C whereby they endothermically undergo oxidation of the carbonate ligand to produce  $Ln_2O_3$  (ESI Figures S30-34). Fourier transform infrared spectrometer in the range 500-4000  $cm^{-1}$ , revealed IR absorptions for what we have assigned as O-H at 3400  $cm^{-1}$ , C-O at 1400  $cm^{-1}$ ,  $Ln-OH$  at 823  $cm^{-1}$ , and  $Ln-OC$  at 705  $cm^{-1}$  (ESI Figures S35-39).

### Magnetic Properties of $LnOHCO_3$

Field cooled (FC) and zero-field cooled (ZFC) magnetic susceptibility data of the  $LnOHCO_3$  frameworks ( $Ln = Gd^{3+}, Tb^{3+}, Dy^{3+}, Ho^{3+}$  and  $Er^{3+}$ ) were measured in a 1000 Oe field from 2 K to 300 K and did not show any indication of long range magnetic order. This data was found to obey Curie-Weiss law over the full temperature range, with the exception of  $DyOHCO_3$  where significant deviations were found to occur above 200 K that likely result from crystal field effects (see Figure 3). Effective magnetic moments were found to be broadly consistent with the values expected for these trivalent lanthanides according to the Russell-Saunders coupling scheme<sup>36</sup> (see Table 2) calculated from mean field Curie-Weiss behaviour (see Figures 3 and S40-S44 for associated fits).

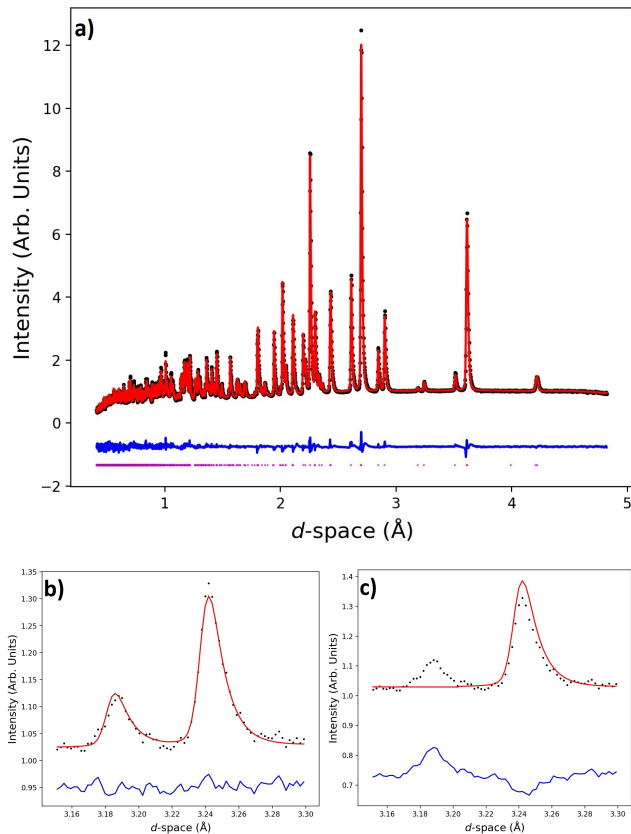


**Figure 2.** Neutron diffraction patterns of TbODCO<sub>3</sub> at 100 K from banks 5 & 6 of the WISH diffractometer. a) Rietveld fit in  $P2_12_12_1$  space group, b) close up of the (102) reflection at 3.18 Å, and correct fitting using  $P2_12_12_1$  space group –  $R_p$ ,  $R_{wp}$  and  $\chi^2$  of fit = 0.0173, 0.0252 and 16.09 respectively, c) close up of Rietveld fit in  $Pnma$  showing systematically absent (012) reflection in  $Pnma$  –  $R_p$ ,  $R_{wp}$  and  $\chi^2$  of fit = 0.0224, 0.0426 and 45.98 respectively. Black crosses, red line, blue line and purple markers indicate the data, calculated intensity, difference plot and position of the Bragg markers, respectively.

**Table 2.** Summary of Curie-Weiss temperatures and magnetic moments for lanthanides in  $LnOHCO_3$ .

Ln	Curie-Weiss Temperature (K)	Magnetic Moment ( $\mu_B$ )
Gd	0.93	7.29
Tb	-5.04	9.30
Dy	-0.84	10.96
Ho	-3.83	10.43
Er	-7.47	9.61

Curie-Weiss temperatures were determined and suggest moderate antiferromagnetic interactions in all materials with the exception of GdOHCO<sub>3</sub>. Aside from Gd, however, the depopulation of Stark levels at lower temperatures in lanthanides with significant orbital angular momentum means that these Curie-Weiss temperatures must be considered tentatively.<sup>37</sup>

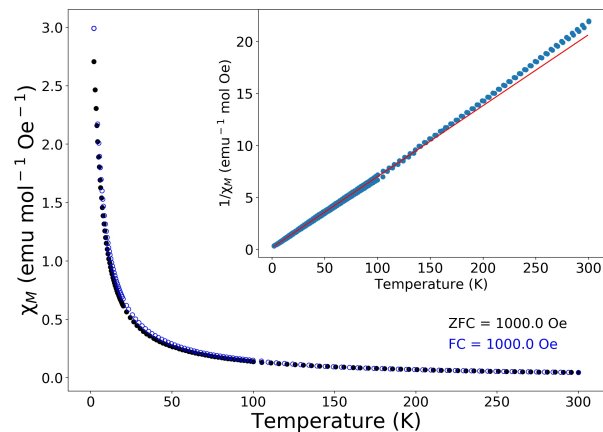


**Figure 3.** DyOHCO<sub>3</sub> FC and ZFC measurements in a 1000 Oe field, the insert shows a Curie-Weiss fit to the inverse magnetic susceptibility measurements below 150 K extrapolated to higher temperature.

Isothermal magnetization measurements on the  $LnOHCO_3$  frameworks measured at 2 K (see Figure 4) reveals that both TbOHCO<sub>3</sub> and DyOHCO<sub>3</sub> are easily magnetized under modest applied fields, with both close to saturation under applied fields of 10 kOe. In contrast, the other frameworks, including GdOHCO<sub>3</sub> continue to magnetize with applied magnetic field up to 50 kOe. The greater ease of magnetization in TbOHCO<sub>3</sub> and DyOHCO<sub>3</sub> of the frameworks in low applied fields is the source of their high MCE performance in fields below 20 kOe, as discussed below. The saturation value of the magnetisation can provide some insight into whether a magnetic material is a Ising or Heisenberg system, in which cases limits of  $g_J/2$  and  $g_J$  are expected<sup>17,38–40</sup>. The magnetic saturation of Gd approaches 7  $\mu_B$ , consistent with a Heisenberg cation, while those of Ho and Er approach values expected in a purely Ising case. Those for DyOHCO<sub>3</sub> and TbOHCO<sub>3</sub> are close to the limit expected for the magnetic cations in an Ising case but are above this suggesting other contributions to the magnetic observed saturation value.

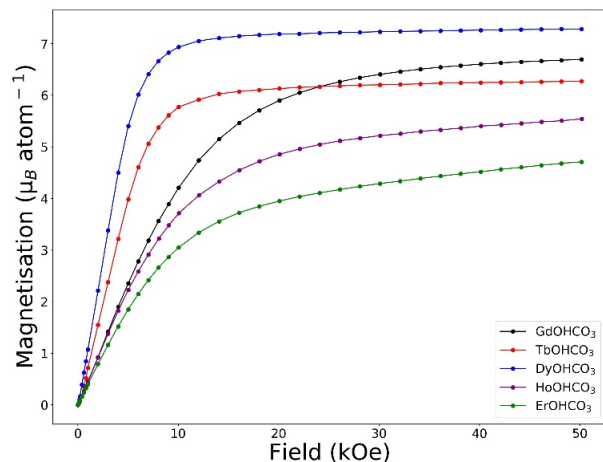


**Figure 4.** Isothermal magnetization measurements on the  $LnOHCO_3$  frameworks measured at 2 K.

Magnetic entropy change,  $\Delta S_m$ , was calculated from the Maxwell relation  $\Delta S_m(T) = \int [\partial M(T, B) / \partial T]_B dB$  - between 2 to 10 K and for field changes between 0 and 1-5 T (see Figures

S45-S50 for magnetization plots). While this is an indirect way of measuring the magnetocaloric effect recent work on  $\text{Gd}(\text{HCO}_2)_3$  and  $\text{GdOHCO}_3$ , have shown that for similar frameworks excellent agreement is usually obtained between this approach and the direct determination of  $\Delta S_m$  from heat capacity measurements.<sup>6,23</sup> The  $\Delta S_m^{\text{max}}$  values determined from this approach are presented in Table 2.

**Table 3. Summary of the peak MCE ( $-\Delta S_m^{\text{max}}$ ) at peak temperatures ( $T_{\text{Max}}$ ) of the studied  $\text{LnOHCO}_3$  at different field changes.**

<i>Ln</i>	$T_{\text{Max}}$ (K)	$\Delta B = 1-0$ T		$\Delta B = 2-0$ T		$\Delta B = 5-0$ T	
		$J \text{ Kg}^{-1} \text{ K}^{-1}$	$\text{mJ cm}^{-3} \text{ K}^{-1}$	$J \text{ Kg}^{-1} \text{ K}^{-1}$	$\text{mJ cm}^{-3} \text{ K}^{-1}$	$J \text{ Kg}^{-1} \text{ K}^{-1}$	$\text{mJ cm}^{-3} \text{ K}^{-1}$
<b>Gd</b>	2	19.32	103.37	44.17	236.31	69.33	370.42
<b>Tb</b>	4	17.64	95.97	30.99	168.62	33.72	183.40
<b>Dy</b>	4	20.76	115.87	33.34	186.15	34.46	192.42
<b>Ho</b>	4	10.84	61.53	19.85	112.67	24.38	138.36
<b>Er</b>	2	15.04	86.43	28.11	161.51	31.98	183.73

As expected from other lanthanide magnetocaloric materials, the previously reported  $\text{GdOHCO}_3$  is observed to have the greatest  $-\Delta S_m^{\text{max}}$  at 2 K, particularly in multiple tesla magnetic fields (see Figures 5, 6 and S71). For moderate field changes of less than 2 T  $\text{TbOHCO}_3$  and  $\text{DyOHCO}_3$  are found to perform exceptionally well between temperatures of 4 and 10 K with  $-\Delta S_m^{\text{max}}$  at 4 K (Figure 5).  $\text{TbOHCO}_3$  and  $\text{DyOHCO}_3$  have a higher  $-\Delta S_m$  than  $\text{GdOHCO}_3$  at all temperatures between 4 and 10 K for a 2-0 T field change and exhibit a trend that suggests this will continue at higher temperatures. Of these two compounds  $\text{DyOHCO}_3$  has the highest  $-\Delta S_m^{\text{max}}$ , at 4 K, of  $33.34 \text{ J Kg}^{-1} \text{ K}^{-1}$  with  $\text{TbOHCO}_3$  having a  $\Delta S_m^{\text{max}}$  of  $30.99 \text{ J Kg}^{-1} \text{ K}^{-1}$  *c.f.*  $\text{GdOHCO}_3$  which has a  $-\Delta S_m$  of  $29.54 \text{ J Kg}^{-1} \text{ K}^{-1}$  for the equivalent temperature and field change. The difference in the performance of  $\text{TbOHCO}_3$  and  $\text{DyOHCO}_3$  is even greater for  $\Delta B = 1-0$  T where they are observed to have  $-\Delta S_m^{\text{max}}$  of  $17.64 \text{ J Kg}^{-1} \text{ K}^{-1}$  and  $20.76 \text{ J Kg}^{-1} \text{ K}^{-1}$  at 4 K respectively, *c.f.*  $\text{GdOHCO}_3$ , which we find to have an equivalent  $-\Delta S_m$  of  $11.67 \text{ J Kg}^{-1} \text{ K}^{-1}$ . In  $\Delta B = 1-0$  T  $\text{DyOHCO}_3$  outperforms all other  $\text{LnOHCO}_3$  at all temperatures above 3 K, and the  $-\Delta S_m^{\text{max}}$  for  $\text{DyOHCO}_3$  is almost twice the  $-\Delta S_m$  of  $\text{GdOHCO}_3$  at the same temperature.

These results are particularly impressive when compared to the benchmark material GGG or  $\text{Dy}_3\text{Ga}_5\text{O}_{12}$  (DGG). For  $\Delta B = 2-0$  T GGG has a  $-\Delta S_m^{\text{max}} = 17.7 \text{ J Kg}^{-1} \text{ K}^{-1}$  or  $145 \text{ mJ cm}^{-3} \text{ K}^{-1}$  at 1.2 K<sup>23</sup> and DGG has a  $-\Delta S_m^{\text{max}} = 11.64 \text{ J Kg}^{-1} \text{ K}^{-1}$  or  $95 \text{ mJ cm}^{-3} \text{ K}^{-1}$  at 1.2 K, although the performance of DGG is modestly better for a 1-0 T field change and at higher temperatures compared to GGG<sup>15,41</sup>.  $\text{DyOHCO}_3$  however, has a  $-\Delta S_m^{\text{max}} = 33.34 \text{ J Kg}^{-1} \text{ K}^{-1}$  or  $186.15 \text{ mJ cm}^{-3} \text{ K}^{-1}$  at 4 K and retains a greater  $-\Delta S_m$  per weight than GGG's  $-\Delta S_m^{\text{max}}$  up to 8 K.  $\text{TbOHCO}_3$  also maintains a  $-\Delta S_m$  that is higher than GGG's  $\Delta S_m^{\text{max}}$  for  $\Delta B = 2-0$  T between 3-6 K. The MCE performance of  $\text{HoOHCO}_3$  and  $\text{ErOHCO}_3$  are less remarkable. The later continues to decrease on cooling to 2 K but with much poorer performance for a given temperature and applied field change compared to  $\text{GdOHCO}_3$ .  $\text{HoOHCO}_3$ , in contrast has its  $-\Delta S_m^{\text{max}}$  at 4 K but this is much lower than observed for  $\text{DyOHCO}_3$  and  $\text{TbOHCO}_3$ . Thus its  $-\Delta S_m$  only exceeds that of  $\text{GdOHCO}_3$  for  $\Delta B = 1-0$  T and 2-0 T, respectively, above 6 K and 7 K and this is then only by small amounts. Perhaps more notably  $-\Delta S_m$  becomes negative at 2 K, which from the Maxwell relation can be interpreted as indicating that  $\partial M /$

$\partial T$  is becoming negative at low temperatures, consistent with the material being close to a transition to an antiferromagnetic state.

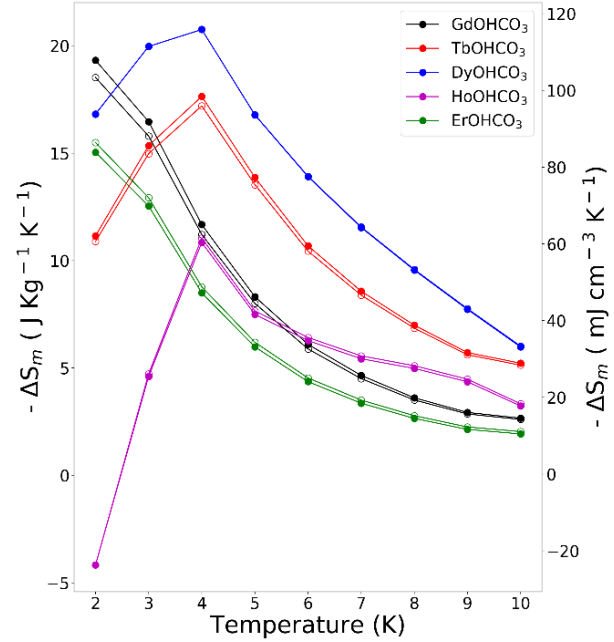


**Figure 5. Magnetic entropy changes for the  $\text{LnOHCO}_3$  series for  $\Delta B = 1-0$  T. The filled and hollow symbols mark mass and volumetric units.**

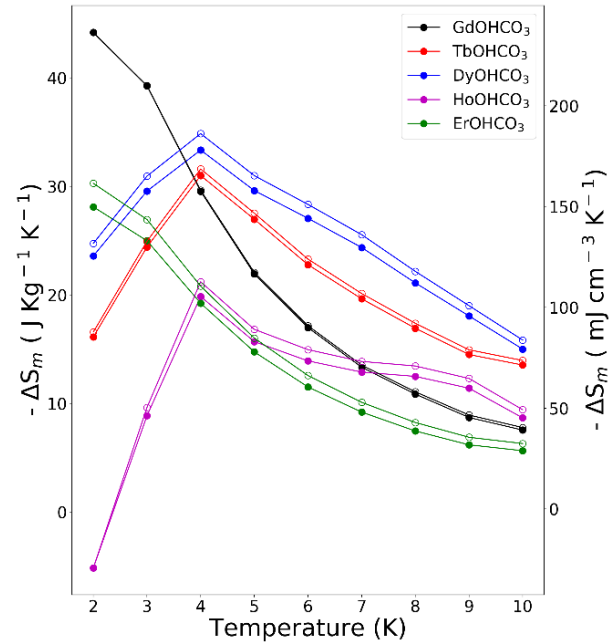


**Figure 6. Magnetic entropy changes for the  $\text{LnOHCO}_3$  series for  $\Delta B = 2-0$  T. The filled and hollow symbols mark mass and volumetric units.**

The results obtained here vary from those obtained from our previous study of the  $\text{Ln}(\text{HCO}_2)_3$  family in two key respects. Firstly in the formates  $\text{Tb}(\text{HCO}_2)_3$  showed the greatest MCE performance<sup>18</sup> between 4-10 K, for applied field changes of less

than 2 T. While  $\text{TbOHCO}_3$  retains qualitatively similar MCE behaviour its performance above 4 K, where for low applied fields it outperforms  $\text{GdOHCO}_3$ , is less than that observed for  $\text{DyOHCO}_3$ . This is distinct from the behaviour of  $\text{Dy}(\text{HCO}_2)_3$ , which continues to increase at low temperatures in a similar fashion but with much lower performance than  $\text{Gd}(\text{HCO}_2)_3$ . Secondly the value of  $-\Delta S_m^{\text{max}}$  for  $\text{TbOHCO}_3$  and  $\text{DyOHCO}_3$  is much closer to that of  $\text{GdOHCO}_3$  (see Table 2) than is the case for  $\text{Tb}(\text{HCO}_2)_3$  compared to  $\text{Gd}(\text{HCO}_2)_3$  (*c.f.*  $8.08 \text{ J Kg}^{-1} \text{ K}^{-1}$  and  $10.64 \text{ J Kg}^{-1} \text{ K}^{-1}$  for 1-0 and 2-0 T field changes in  $\text{Tb}(\text{HCO}_2)_3$  to  $13.23 \text{ J Kg}^{-1} \text{ K}^{-1}$  and  $25.37 \text{ J Kg}^{-1} \text{ K}^{-1}$  for 1-0 and 2-0 T field changes in  $\text{Gd}(\text{HCO}_2)_3$ )<sup>18</sup>. This is related to much larger MCE effects above 4 K in  $\text{TbOHCO}_3$  and  $\text{DyOHCO}_3$  compared to  $\text{Tb}(\text{HCO}_2)_3$ , offering performance comparable to that found in GGG, below 2 K, at higher temperatures for the first time.

In the  $\text{Gd}_{1-x}\text{Tb}_x(\text{HCO}_2)_3$  series doping with up to 40 % Tb improved the MCE effect observed above 4 K without significantly decreasing the performance at lower temperatures.<sup>18</sup> The magnetic properties of doped  $\text{GdOHCO}_3$  with  $\text{Tb}^{3+}$  and  $\text{Dy}^{3+}$  were therefore explored with steps of  $x=0.2$  across the  $\text{Tb}_x\text{Gd}_{1-x}\text{OHCO}_3$  and  $\text{Dy}_x\text{Gd}_{1-x}\text{OHCO}_3$  series. The performance of these doped compounds was found to vary from a physical mix of the end member compounds, suggesting that magnetic coupling between magnetic cations plays a key role in their MCE (see Figure 7; further magnetic property data can be seen in Figures S51-81). In particular there is a sharp change between  $\text{GdOHCO}_3$ -like MCE performance and  $\text{DyOHCO}_3$  and  $\text{TbOHCO}_3$  performance between 40 and 60 % Dy doping and 60 and 80 % Tb doping, respectively. Unfortunately, even a small doping of any of the three end members leads to a significant reduction in  $-\Delta S_m^{\text{max}}$  without any compensating increase in performance at other temperature ranges. Potentially improving the magnetocaloric performance of this family could be explored further using other doping strategies, such as other lanthanide cations or lower doping percentages, but this is beyond the immediate focus of this work.

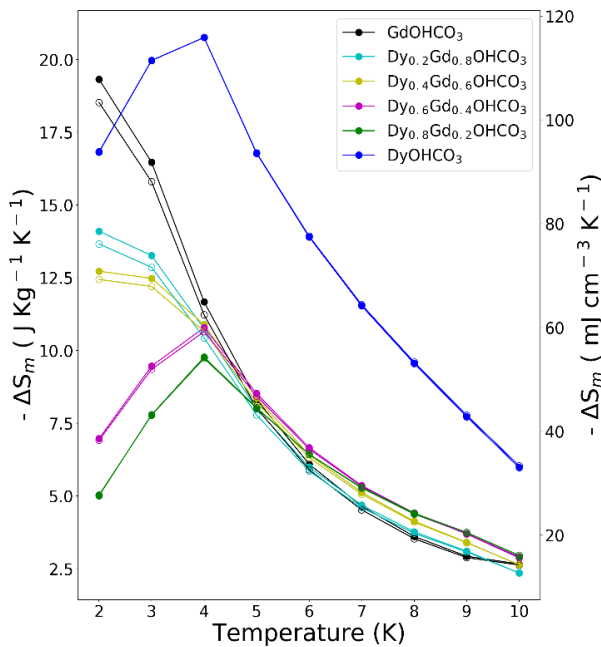


**Figure 7. Magnetic entropy changes for a  $\Delta B = 1-0$  T for  $\text{Dy}_x\text{Gd}_{1-x}\text{OHCO}_3$ . The filled symbols mark this per unit mass and the hollow in volumetric units.**

#### Magnetostructural relationships

There are a number of structural differences between the  $\text{Ln}(\text{HCO}_2)_3$  and  $\text{LnOHCO}_3$  frameworks that could lead to the observed differences in their magnetocaloric properties. Firstly, while the Ln cations in the  $\text{Ln}(\text{HCO}_2)_3$  are in a highly symmetric 9 coordinate tricapped trigonal prism environment with  $3m$  site symmetry those in the  $\text{LnOHCO}_3$  structure have 1 site symmetry, which can be either viewed as a 10-coordinate environment or a highly distorted  $\text{LnO}_8$  square antiprism coordination environment. This difference may influence the magnetic anisotropy<sup>42</sup> and affect the relative ease with which the orbital angular momentum may partially align with the applied magnetic field, effecting the MCE observed. As discussed above the magnetization of  $\text{DyOHCO}_3$  is essentially saturated at 20 kOe at approximately  $7 \mu_B \text{ atom}^{-1}$ , while the magnetization of  $\text{Dy}(\text{HCO}_2)_3$  increases relatively rapidly to about  $5 \mu_B \text{ atom}^{-1}$  by 20 kOe before increasing more slowly to just above  $6 \mu_B \text{ mole}^{-1}$  at 50 kOe, where it is far from saturation<sup>18</sup>. The magnetisation value observed for  $\text{Dy}(\text{HCO}_2)_3$  at low applied fields is close to the expected contribution to the moment expected from a purely Ising ion ( $g_J/2=5 \mu_B \text{ atom}^{-1}$  for  $f^9 \text{ Dy}^{3+}$ ) while that observed for  $\text{DyOHCO}_3$ , as discussed above, is significantly higher than this but well short of that expected from a Heisenberg ion ( $g_J=10 \mu_B \text{ atom}^{-1}$ ). This additional magnetisation in  $\text{DyOHCO}_3$  at such low applied fields is unusual since Dy is typically exhibits Ising anisotropy and is likely to further enhance its MCE properties. This could be interpreted as indicating the alignment of some fraction of the orbital angular momentum with the applied field although this typically requires a very strong field.<sup>43</sup>

Since Dy, which is a Kramer ion, responds very differently between the two series alternating between exhibiting MCE properties qualitatively similar to  $\text{Gd}(\text{HCO}_2)_3$ , which also contains a Kramers ion, and  $\text{TbOHCO}_3$ , which contains a non-Kramers ion, suggests Kramer ion effects do not primarily determine which systems have MCE maximised below or above 4 K. That Tb and Ho containing members of both  $\text{LnOHCO}_3$  and  $\text{Ln}(\text{HCO}_2)_3$  have MCE optimised for use above 4 K may suggest non-Kramers ions more commonly have MCE of this type, although it is notable that, for example,  $\text{A}_3\text{Ga}_5\text{O}_{12}$  ( $A = \text{Tb}$  or  $\text{Ho}$ ) do not<sup>41</sup> so the relevance of this is far from clear.

Another factor that likely effects the magnetic properties of these two families of materials is the different ways in which the cations in their structures are connected, which will play a key role in their magnetic coupling. The structure of  $\text{Ln}(\text{HCO}_2)_3$  can be readily simplified into face-sharing chains packed into a frustrated triangular lattice and it has been argued that the combination of low dimensionality and magnetic frustration plays a key role in the magnetocaloric properties of this family.<sup>18,19</sup> In particular, the high magnetocaloric performance of  $\text{Tb}(\text{HCO}_2)_3$  above 4 K in low applied magnetic fields has been attributed to the presence of ferromagnetic coupling within chains with complete magnetic order suppressed by the frustrated coupling between chains<sup>18,19</sup>. As discussed above the  $\text{LnOHCO}_3$  frameworks structure is more complex and can be viewed as either consisting of face-sharing chains of  $\text{LnO}_{10}$  polyhedra running along the  $b$ -axis or zig-zag chains of  $\text{LnO}_8$  polyhedra along the  $a$ -axis. Density-Functional Theory calculations by Chen *et al.*<sup>23</sup>, on  $\text{GdOHCO}_3$  suggested the presence of dominant antiferromagnetic coupling within the face-sharing chains ( $J_1$  in Figure 8), with frustrated antiferromagnetic coupling between them ( $J_2$  and  $J_3$ ). This is consistent with the shortest superexchange pathway being through the hydroxide oxygen atom along the  $b$ -axis, such that coupling between face-sharing chains of  $\text{LnO}_{10}$  polyhedra may dominate even if the other two superexchange pathways along such chains are longer than others in this material. While dipole-dipole magnetic coupling can also be significant quantifying these interactions for a particular structure requires further analysis, which was omitted by the

previous study of Chen *et al.*<sup>23</sup> and is beyond the data presented in this work.

Direct analysis of the magnetic interactions in the  $LnOHCO_3$  frameworks is, however, required to confirm this or whether additional interactions, such as through  $J_4$  which couples neighbouring chains diagonally, is needed to which magnetic interactions are dominant in the paramagnetic phase of the complex  $LnOHCO_3$  structure and how these affect the MCE of this family of compounds. While this is beyond the scope of this work, which focuses primarily on the bulk MCE properties of these compounds preliminary neutron scattering measurements show that those compounds with MCE properties optimized above 4 K exhibit the evolution of structured magnetic diffuse scattering below 20 K (see Figure 9 and S82-84). This supports the existence of significant local magnetic correlations in these compounds, consistent with the expected existence of low dimensional and frustrated magnetic coupling in these compounds given the lack of any long range magnetic order to 2 K.

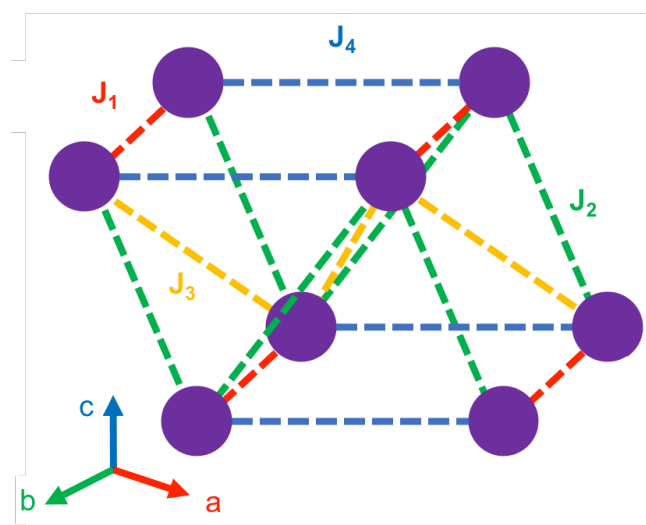


Figure 8. Diagram of  $J$  interactions shown from (111) plane.  $Ln$  in purple and  $J$  interactions colour coordinated.

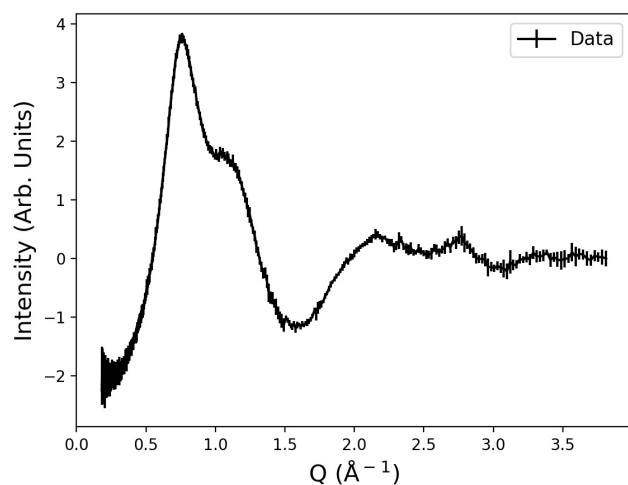


Figure 9. Diffuse scattering of  $TbODCO_3$  at 1.5 K, caused by magnetic frustration

#### 4. CONCLUSIONS

In this study neutron powder and X-ray single crystal diffraction has indicated that the  $LnOHCO_3$  (where  $Ln = Gd^{3+}$ ,  $Tb^{3+}$ ,  $Dy^{3+}$ ,  $Ho^{3+}$  and  $Er^{3+}$ ) frameworks adopt an orthorhombic  $P2_12_12_1$

structure through all the temperature range studied, resolving previous reports that they may alternatively adopt  $Pnma$  symmetry<sup>23,26</sup>. The MCE of  $LnOHCO_3$  compounds containing heavier lanthanides, Tb-Er, have also been analysed for the first time, with these materials found to remain paramagnetic to 2 K. We have shown that, although the  $-\Delta S_m^{\max}$  of the other lanthanides for high applied fields is not as great as  $GdOHCO_3$ , the temperature at which the performance of  $TbOHCO_3$  and  $DyOHCO_3$  peaks is significantly higher; as a result in applied fields of less than 20 kOe, the maximum field typically achievable with permanent magnets, these compounds have significantly higher MCE than  $GdOHCO_3$  above 4 K.  $DyOHCO_3$ , which exhibits the highest MCE performance in this régime, has a greater  $-\Delta S_m^{\max}$  than the benchmark materials  $Gd_3Ga_5O_{12}$  and  $Dy_3Ga_5O_{12}$  with peak performance shifted to higher temperatures. It appears likely that both the local environment of the magnetic cation and the short-range interactions between these materials seem to be playing an important role in the efficiency of the materials. This makes it a possible replacement for liquid helium cooling, with the highest MCE above 4 K of any paramagnetic cooling material.

#### ASSOCIATED CONTENT

##### Supporting Information

Electronic supplementary information (ESI) available: CIFs from single crystal X-ray structure determination and figures displaying further crystallographic details, powder diffraction patterns, magnetic property measurements, infrared spectra and thermogravimetric analysis are available. For ESI and crystallographic data in CIF or other electronic format.

#### AUTHOR INFORMATION

##### Corresponding Author

\*School of Physical Sciences, Ingram Building, University of Kent, Canterbury, CT2 7NH, UK. E-mail: P.Saines@kent.ac.uk

##### Author Contributions

The manuscript was written through contributions of all authors.

##### Funding Sources

The authors would like to thank the Science and Technologies Facilities Council for access to the ISIS facility at Harwell. RJCD would like to thank the University of Kent's for financial support through the provision of a Vice-Chancellors scholarship.

#### ACKNOWLEDGMENT

We would like to thank Dr. Pascal Manuel for his assistance with neutron diffraction measurements.

#### REFERENCES

- (1) Smith, A. Who Discovered the Magnetocaloric Effect? *Eur. Phys. J. H* **2013**, *38*, 507–517.
- (2) Spichkin, Y. I.; Zvezdin, A. K.; Gubin, S. P.; Mischenko, A. S.; Tishin, A. M. Magnetic Molecular Clusters as Promising Materials for Refrigeration in Low-Temperature Regions. *J. Phys. D. Appl. Phys.* **2001**, *34*, 1162–1166.
- (3) Evangelisti, M.; Brechin, E. K.; Verdaguer, M. Recipes for Enhanced Molecular Cooling. *Dalt. Trans.* **2010**, *39*, 4672–4676.
- (4) Zheng, Y.-Z.; Zhou, G.-J.; Zheng, Z.; Winpenny, R. E. P. Molecule-Based Magnetic Coolers. *Chem. Soc. Rev.* **2014**, *43*, 1462–1475.
- (5) Sharples, J. W.; Collison, D. Coordination Compounds and the Magnetocaloric Effect. *Polyhedron* **2013**, *54*, 91–103.
- (6) Lorusso, G.; Sharples, J. W.; Palacios, E.; Roubeau, O.; Brechin, E. K.; Sessoli, R.; Rossin, A.; Tuna, F.; McInnes, E. J. L.;

- Collison, D.; et al. A Dense Metal-Organic Framework for Enhanced Magnetic Refrigeration. *Adv. Mater.* **2013**, *25*, 4653–4656.
- (7) Lvovsky, Y.; Stautner, E. W.; Zhang, T. Novel Technologies and Configurations of Superconducting Magnets for MRI. *Supercond. Sci. Technol.* **2013**, *26*, 93001.
- (8) Radebaugh, R. Cryocoolers: The State of the Art and Recent Developments. *J. Phys. Condens. Matter* **2009**, *21*, 164219–164227.
- (9) Gan, Z. H.; Dong, W. Q.; Qiu, L. M.; Zhang, X. B.; Sun, H.; He, Y. L.; Radebaugh, R. A Single-Stage GM-Type Pulse Tube Cryocooler Operating at 10.6K. *Cryogenics* **2009**, *49*, 198–201.
- (10) Chen, L.; Jin, H.; Wang, J.; Zhou, Y.; Zhu, W.; Zhou, Q. 18.6 K Single-Stage High Frequency Multi-Bypass Coaxial Pulse Tube Cryocooler. *Cryogenics* **2013**, *54*, 54–58.
- (11) Paddison, J. A. M.; Jacobsen, H.; Petrenko, O. A.; Fernández-Díaz, M. T.; Deen, P. P.; Goodwin, A. L. Hidden Order in Spin-Liquid Gd<sub>3</sub>Ga<sub>5</sub>O<sub>12</sub>. *Science* **2015**, *350*, 179–181.
- (12) Barclay, J. A.; Steyert, W. A. Materials for Magnetic Refrigeration between 2 K and 20 K. *Cryogenics* **1982**, *22*, 73–80.
- (13) Palacios, E.; Rodríguez-Velamazán, J. A.; Evangelisti, M.; McIntyre, G. J.; Lorusso, G.; Visser, D.; De Jongh, L. J.; Boatner, L. A. Magnetic Structure and Magnetocalorics of GdPO<sub>4</sub>. *Phys. Rev. B* **2014**, *90*, 214423.
- (14) Silva, R. S.; Barrozo, P.; Moreno, N. O.; Aguiar, J. A. Structural and Magnetic Properties of LaCrO<sub>3</sub> Half-Doped with Al. *Ceram. Int.* **2016**, *42*, 14499–14504.
- (15) Numazawa, T.; Kamiya, K.; Okano, T.; Matsumoto, K. Magneto Caloric Effect in (Dy<sub>x</sub>Gd<sub>1-x</sub>)<sub>3</sub>Ga<sub>5</sub>O<sub>12</sub> for Adiabatic Demagnetization Refrigeration. *Physica B* **2003**, *329–333*, 1656–1657.
- (16) Mukherjee, P.; Wu, Y.; Lampronti, G. I.; Dutton, S. E. Magnetic Properties of Monoclinic Lanthanide Orthoborates, LnBO<sub>3</sub>, Ln = Gd, Tb, Dy, Ho, Er, Yb. *Mater. Res. Bull.* **2018**, *98*, 173–179.
- (17) Mukherjee, P.; Dutton, S. E. Enhanced Magnetocaloric Effect from Cr Substitution in Ising Lanthanide Gallium Garnets Ln<sub>2</sub>CrGa<sub>4</sub>O<sub>12</sub> (Ln = Tb, Dy, Ho). *Adv. Funct. Mater.* **2017**, *27*, 1701950.
- (18) Saines, P. J.; Paddison, J. A. M.; Thygesen, P. M. M.; Tucker, M. G. Searching beyond Gd for Magnetocaloric Frameworks: Magnetic Properties and Interactions of the Ln(HCO<sub>2</sub>)<sub>3</sub> Series. *Mater. Horiz.* **2015**, *2*, 528–535.
- (19) Harcombe, D. R.; Welch, P. G.; Manuel, P.; Saines, P. J.; Goodwin, A. L. One-Dimensional Magnetic Order in the Metal-Organic Framework Tb(HCOO)<sub>3</sub>. *Phys. Rev. B* **2016**, *94*, 174429.
- (20) Chen, Y.-C.; Prokleška, J.; Xu, W.-J.; Liu, J.-L.; Liu, J.; Zhang, W.-X.; Jia, J.-H.; Sechovský, V.; Tong, M.-L. A Brilliant Cryogenic Magnetic Coolant: Magnetic and Magnetocaloric Study of Ferromagnetically Coupled GdF<sub>3</sub>. *J. Mater. Chem. C* **2015**, *3*, 12206–12211.
- (21) Biswas, S.; Jena, H. S.; Adhikary, A.; Konar, S. Two Isostructural 3D Lanthanide Coordination Networks (Ln = Gd<sup>3+</sup>, Dy<sup>3+</sup>) with Squashed Cuboid-Type Nanoscopic Cages Showing Significant Cryogenic Magnetic Refrigeration and Slow Magnetic Relaxation. *Inorg. Chem.* **2014**, *53*, 3926–3928.
- (22) Michiba, K.; Miyawaki, R.; Minakawa, T.; Terada, Y.; Nakai, I.; Matsubara, S. Crystal Structure of Hydroxylbastnasite-(Ce) from Kamihouri, Miyazaki Prefecture, Japan. *J. Mineral. Petrol. Sci.* **2013**, *108*, 326–334.
- (23) Chen, Y.-C.; Qin, L.; Meng, Z.-S.; Yang, D.-F.; Wu, C.; Fu, Z.; Zheng, Y.-Z.; Liu, J.-L.; Tarasenko, R.; Orendáč, M.; et al. Study of a Magnetic-Cooling Material Gd(OH)CO<sub>3</sub>. *J. Mater. Chem. A* **2014**, *2*, 9851–9858.
- (24) Tahara, T.; Nakai, I.; Miyawaki, R.; Matsubara, S. Crystal Chemistry of RE(CO<sub>3</sub>)OH. *Z. Kristallogr.* **2007**, *222*, 326–334.
- (25) Michiba, K.; Tahara, T.; Nakai, I.; Miyawaki, R.; Matsubara, S. Crystal Structure of Hexagonal RE(CO<sub>3</sub>)OH. *Z. Kristallogr.* **2011**, *226*, 518–530.
- (26) Sheu, H.-S.; Shih, W.-J.; Chuang, W.-T.; Li, I.-F.; Yeh, C.-S. Crystal Structure and Phase Transitions of Gd(CO<sub>3</sub>)OH Studied by Synchrotron Powder Diffraction. *J. Chinese Chem. Soc.* **2010**, *57*, 938–945.
- (27) Daudin, B.; Lagnier, R.; Salce, B. Thermodynamic Properties of the Gadolinium Gallium Garnet, Gd<sub>3</sub>Ga<sub>5</sub>O<sub>12</sub>, between 0.05 and 25 K. *J. Magn. Magn. Mater.* **1982**, *27*, 315–322.
- (28) B. Hunter. Rietica - A Visual Rietveld Program. *Int. Union Crystallogr., Comm. Powder Diffr. Newsl.* **1998**, *20*, 21.
- (29) A.C. Larson and R.B. Von Dreele. General Structure Analysis System (GSAS). *Los Alamos Natl. Lab. Rep. LAUR* **2000**, 86–748.
- (30) Toby, B. H.; Hall, S.; Allen, F.; Brown, I.; Rietveld, H. EXPGUI, a Graphical User Interface for GSAS. *J. Appl. Crystallogr.* **2001**, *34*, 210–213.
- (31) Agilent (2016). CrysAlis PRO. Agilent Technologies Ltd. CrysAlis PRO. Yarnton, Oxfordshire, England Version 171.38.41. Agilent Technologies Ltd: Yarnton, Oxfordshire, England.
- (32) Sheldrick, G. M. A Short History of SHELX. *Acta Crystallogr. Sect. A Found. Crystallogr.* **2008**, *64*, 112–122.
- (33) Sheldrick, G. M. Crystal Structure Refinement with SHELXL. *Acta Crystallogr. Sect. C Struct. Chem.* **2015**, *71*, 3–8.
- (34) Dolomanov, O. V.; Bourhis, L. J.; Gildea, R. J.; Howard, J. A. K.; Puschmann, H. OLEX2: A Complete Structure Solution, Refinement and Analysis Program. *J. Appl. Crystallogr.* **2009**, *42*, 339–341.
- (35) Brese, N. E.; O’Keeffe, M.; IUCr. Bond-Valence Parameters for Solids. *Acta Crystallogr. Sect. B Struct. Sci.* **1991**, *47*, 192–197.
- (36) Russell, H. N.; Saunders, F. A. New Regularities in the Spectra of the Alkaline Earths. *Astrophys. J.* **1925**, *61*, 38–69.
- (37) Van Vleck, J. H. *The Theory of Electric and Magnetic Susceptibilities*; Oxford University Press: Oxford, 1965.
- (38) Filippi, J.; Tcheou, F.; Rossat-Mignod, J. Crystal Field Effect on the Paramagnetic Properties of Dy<sup>3+</sup> Ion in Dysprosium Gallium Garnet. *Solid State Commun.* **1980**, *33*, 827–832.
- (39) Reid, B. L.; McMorro, D. F.; Mitchell, P. W.; Prakash, O.; Murani, A. P. Crystal Field for Ho<sup>3+</sup> in Holmium Gallium Garnet. *Physica B* **1991**, *174*, 51–55.
- (40) Hammann, J.; Ocio, M. Magnetic Ordering Induced by Hyperfine Interactions in the Terbium and Holmium Gallium Garnets. *Physica B & C* **1977**, *86–88*, 1153–1155.
- (41) Mukherjee, P.; Sackville Hamilton, A. C.; Glass, H. F. J.; Dutton, S. E. Sensitivity of Magnetic Properties to Chemical Pressure in Lanthanide Garnets Ln<sub>3</sub>A<sub>2</sub>X<sub>3</sub>O<sub>12</sub>, Ln = Gd, Tb, Dy, Ho, A = Ga, Sc, In, Te, X = Ga, Al, Li. *J. Phys. Condens. Matter* **2017**, *29*, 405808.
- (42) Chilton, N. F.; Collison, D.; McInnes, E. J. L.; Winpenny, R. E. P.; Soncini, A. An Electrostatic Model for the Determination of Magnetic Anisotropy in Dysprosium Complexes. *Nat. Commun.* **2013**, *4*, 2551–2557.
- (43) Spaldin, N. A. *Magnetic Materials: Fundamentals and Applications*. In *Magnetic Materials: Fundamentals and Applications*; Cambridge University Press: Cambridge, 2010; p 37.

## Table of Contents artwork

